# A DYNAMIC PROCEDURE FOR ADVANCED SUBGRID-SCALE MODELS AND WALL-BOUNDED FLOWS

**Baya Toda Hubert**
Energy Applications Techniques
IFP Energie Nouvelles
Rueil - Malmaison, France
hubert.baya-toda@ifpen.fr

**Olivier Cabrit**
Department of Mechanical Engineering
University of Melbourne
Victoria 3010, Australia
o.cabrit@unimelb.au

**Karine Truffin**
Energy Applications Techniques
IFP Energie Nouvelles
Rueil - Malmaison, France
karine.truffin@ifpen.fr

**Bruneaux Gilles**
Energy Applications Techniques
IFP Energie Nouvelles
Rueil - Malmaison, France
gilles.bruneaux@ifpen.fr

**Franck Nicoud**
CNRS I3M 5149
University Montpellier II
Montpellier, France
franck.nicoud@univ-montp2.fr

## ABSTRACT

Large Eddy Simulations (LES) in complex geometries require advanced models able to take into account the properties of the turbulence, variations of the mesh resolution and the accuracy of numerical schemes. In this study, a recently developed subgrid scale (SGS) model that takes into account several properties of the turbulence is used and combined with a global dynamic procedure suitable for such an advanced SGS model. A modification is introduced into the global procedure to account for solid boundaries. Validations are first performed on academic cases: an homogeneous isotropic turbulence and a turbulent channel. In addition, the potential of this global dynamic formulation is investigated on a more complex experimental test case performed at IFPEn. This test case corresponds to an hot unsteady impinging jet in presence of a cold cross flow. The resulting model gives fairly good results on the different configurations and does not require any homogeneous directions nor clipping.

## INTRODUCTION

One way to overcome the drawbacks of the Smagorinsky (Smagorinsky, 1963) model is to use the Germano-identity (Germano *et al.*, 1991) with Lilly correction (Lilly, 1992). The constant of the Smagorinsky model is evaluated dynamically in order to adapt the SGS dissipation to the numerics (mesh refinement/numerical scheme) and to the flow features. To avoid local negative values leading to numerical instabilities, the constant is averaged over homogeneous directions. This procedure was proved to give very good results in simple configurations like in homogeneous isotropic turbulence (HIT) or in turbulent channel flows but it is almost impossible to apply it to complex geometries like piston engines or wind turbines. The development of more advanced models like the WALE (Nicoud and Ducros , 1999) and the Vreman (Vreman, 2004) models gives now the possibility to evaluate the model's constant globally rather than locally. Because the operators which they are based on go to zero in multiple cases where the SGS activity is not expected to be present, it remains to estimate their global dissipation. A recent study (Lee *et al.*, 2010) showed that the most efficient and easy to implement global dynamic procedure consists in performing a volume weighted averaging of local values that are obtained through the Germano identity. However, this procedure does not take into account the effect of solid boundaries that can alter the predictions of the global procedure. The objective of this study is then to improve the global dynamic procedure in order to take into account the presence of solid boundaries. The procedure will be applied to the sigma model: $\sigma$-model (Nicoud *et al.*, 2011, Baya Toda *et al.*, 2010). In addition to have the proper cubic near wall behavior, it also vanishes for different type of laminar flows where no SGS activity is expected: 2D flows and isotropic contraction and expansion. Due to this properties, the $\sigma$-model is more suitable than the WALE and Vreman models for the global dynamic procedure. One can also expect that the proposed modification of the global procedure can be applied to the previously cited models.

The paper is organized as follows: in section 1, the governing equations and the different SGS models (dynamic/static) are presented. In section 2, validation tests are performed on the HIT of Comte-Bellot and Corsin (Comte-Bellot and Corsin, 1971) and on a turbulent channel flow (Moser *et al.*, 1999) at friction Reynolds number $Re_\tau = 395$. The later case illustrates that the volume averaging of the global constant is not appropriate for wall-bounded flows. Better results are then obtained thanks to improved averaging procedure where the near wall regions are automatically accounted for. In this view, the volume averaging is weighted by a dimensionless sensor which vanishes in regions where shear dominates rotation (Baya Toda *et al.*, 2010). The potential of the global procedure is further investigated on a more complex case that consists of an impinging hot jet in a cross flow presented in

section 3. The experiment is set up at IFP En. Numerical results are compared with PIV measurements. This section is followed by a general conclusion.

## GOVERNING EQUATION AND SUBGRID-SCALE MODELS

The filtered compressible Navier-Stokes equations are solved in this study but their incompressible counterpart are presented here for simplicity since only low Mach number flows will be considered:

$$\frac{\partial u_j}{\partial x_j} = 0 \tag{1}$$

$$\frac{\partial u_i}{\partial t} + \frac{\partial (u_i u_j)}{\partial x_j} = -\frac{1}{\rho}\frac{\partial p}{\partial x_i} + \nu \frac{\partial^2 u_i}{\partial x_i \partial x_j} + \frac{\partial \tau_{ij}^{sgs}}{\partial x_j} + S_i \tag{2}$$

the grid based filter is omitted for clarity, $u_i$ is the filtered velocity, $t$ is the time, $p$ the pressure, $\rho$ the density, $\nu$ the kinematic viscosity, $S_i$ a source term acting in $i$-direction and $\tau_{ij}^{sgs}$ the subgrid scale (SGS) tensor expressed as:

$$\tau_{ij}^{sgs} = u_i u_j - \overline{u_i u_j} \tag{3}$$

Eddy viscosity models will be considered only in this study to model the SGS tensor which then takes the form:

$$\tau_{ij}^{sgs} - \frac{1}{3}\tau_{kk}^{sgs}\delta_{ij} = 2\nu_{SGS} S_{ij} \tag{4}$$

where $S_{ij}$ is the strain rate based on the filtered velocity $u_i$ and $\nu_{SGS}$ the eddy viscosity.

### The dynamic Smagorinsky model

The dynamic Smagorinsky model is based on the Germano-identity and is expressed as:

$$\nu_{\mathrm{SGS}} = (C_s\Delta)^2\, \mathscr{D}_s \;;\; \mathscr{D}_s = \sqrt{2S_{ij}S_{ij}} \tag{5}$$

The model constant $C_s$ is computed from:

$$(C_s\Delta)^2 = \max\left[-\frac{\langle L_{ij}M_{ij}\rangle_{\mathrm{loc}}}{2\langle M_{ij}M_{ij}\rangle_{\mathrm{loc}}}, 0\right] \tag{6}$$

where $L_{ij} = \widetilde{u_i}\,\widetilde{u_j} - \widetilde{u_i}\,\widetilde{u_i}$ is the Leonard term based on the grid based filter and test filter $\widetilde{\cdot}$. Besides, $M_{ij}$ is directly related to the differential of the model:

$$M_{ij} = \frac{\widetilde{\Delta}^2}{\Delta^2}\widetilde{\mathscr{D}_s}\widetilde{S_{ij}} - \widetilde{\mathscr{D}_s\, S_{ij}},$$

where $\widetilde{\Delta}$ stands for the test filter width. In addition, $\langle\cdot\rangle_{\mathrm{loc}}$ stands for an integral taken over a small volume (typically a few grid cells) surrounding the current grid point and the model constant depends on both space and time. The local dynamic Smagorinsky model is referred to as the SMD model in this paper.

### Advanced static model

In the following, "advanced" models stands for static SGS models with the desirable property that they produce zero eddy-viscosity near solid-boundaries. Examples of such models are the Vreman (Vreman, 2004) and the WALE (Nicoud and Ducros , 1999) models that respectively vanish with a linear and cubic behavior in pure shear regions.

As emphasized in the introduction, the chosen advanced model is the $\sigma$-model. It is based on the singular values of the velocity gradient tensor. It has the interesting properties to vanish in 2D flows 2D axisymmetric and 3D isotropic expansion/contraction. These are examples of flows where no SGS activity is expected. In addition, it has the proper $y^3$ asymptotic behavior near solid boundaries. The $\sigma$-model eddy viscosity is expressed as:

$$\nu_{\mathrm{SGS}} = (C_\sigma\Delta)^2\, \mathscr{D}_\sigma \;;\; \mathscr{D}_\sigma = \frac{\sigma_3(\sigma_1-\sigma_2)(\sigma_2-\sigma_3)}{\sigma_1^2} \tag{7}$$

where $\sigma_1 \geq \sigma_2 \geq \sigma_3 \geq 0$ are the three singular values of $g_{ij}$ the velocity gradient tensor. $C_\sigma = 1.5$.

### Global dynamic procedure

The model eddy viscosity is expressed from Eq.7 and the model constant $C_\sigma^{Gvol}$ is evaluated from:

$$\left(C_\sigma^{Gvol}\Delta\right)^2 = -\frac{\left\langle L_{ij}M_{ij}^\sigma\right\rangle_{\mathrm{vol}}}{2\left\langle M_{ij}^\sigma M_{ij}^\sigma\right\rangle_{\mathrm{vol}}}; \tag{8}$$

$M_{ij}^\sigma$ is obtained by replacing $\mathscr{D}_s$ by $\mathscr{D}_\sigma$ in the expression of $M_{ij}$. $\langle\cdot\rangle_{\mathrm{vol}}$ stand for a volume averaging over the entire domain. The contribution of each cell in the average is weighted by its volume. The resulting constant is then homogeneous in space and varies only in time. This model is referred to as the GSIG model throughout this paper.

### Modified global dynamic procedure

The basic idea behind this modification is to remove near wall regions from the evaluation of the global constant. Indeed, close to the wall, the terms $L_{ij}M_{ij}$ and $M_{ij}M_{ij}$ are high and can be even higher than their values in the center of the channel. Since only viscous effects are dominant near the wall, it is then necessary in order to have the appropriate estimation of the mean constant to keep only values that are not in the near wall region. This consist in weighting each contribution by a sensor that vanishes in those regions. The chosen sensor in our case is the SVS sensor inspired from the WALE model but one can suppose that another sensor that vanishes

in shear region could also be used (for example the dimensionless sigma operator $\frac{\mathscr{D}_\sigma}{\sigma_1}$). The SVS is expressed as :

$$SVS = \frac{(S_{ij}^d S_{ij}^d)^{3/2}}{(S_{ij}^d S_{ij}^d)^{3/2} + (S_{ij}S_{ij})^3} \tag{9}$$

where $S_d^{ij}$ is the traceless part of the square of the gradient tensor. It can be easily demonstrated that the SVS takes the values one and zero respectively for pure rotating flows and for pure shear flow with a $y^3$ near wall behavior. The global constant can then be rewritten as followed:

$$\left(C_\sigma^{Gsvs}\Delta\right)^2 = -\frac{\left\langle L_{ij}M_{ij}^\sigma \right\rangle_{\text{svs}}}{2\left\langle M_{ij}^\sigma M_{ij}^\sigma \right\rangle_{\text{svs}}} \tag{10}$$

where $\langle\cdot\rangle_{\text{svs}}$ stands for a global averaging where each cell contribution is weighted by its SVS. The model is referred to as the GsvsSIG model throughout the paper.

All the results presented in this paper were obtained with the AVBP code (AVBP, 2011). The academic test cases were performed with a centered Galerkin finite element method $4^{th}$ order in space with a $3^{rd}$ order Runge-Kutta temporal integration.

## Validation on academic test cases

Simulations of the HIT of CBC are first performed in order to validate the dissipative behavior of the two global models. This is a standard test case where three spectra at three different adimensionnal time 42, 98, 171 are known from the experiment. The objective is to reproduce the proper energy decay rate (as well as the spectra decay) when starting the simulation with the spectrum at time $t^* = 42$. Fig. 1 shows that both models correctly reproduce the energy decay. As expected, for flows without solid boundaries the predictions of the two global models are similar. This is confirmed by the time evolution of the two global constant shown on Fig. 2.

In order to assess the performance of the different models when dealing with solid boundaries, simulation of a turbulent channel flow are also performed at a friction Reynolds number equal to $Re_\tau = 395$. The reference case is the DNS of Moser *et al.* The mesh characteristics were twice larger than the advised minimum channel (Kim and Moin,1987) dimensions. The chosen dimensions were proved to be sufficient to well recover first order statistics (Cabrit and Nicoud, 2009). The later were accumulated over approximately 10 diffusion times. Fig. 3 shows that the results of the modified global dynamic procedure are in good agreement with the DNS. In contrary, the mean velocity predicted by the dynamic Smagorinsky model and the classical global dynamic procedure are overestimated. This is respectively due to the non averaging over the homogeneous direction and to the global volume averaging that is not appropriate when dealing with wall-bounded flows. The later overpredicts the constant that leads to an overprediction of the SGS viscosity as shown on Fig. 4. In contrary, by giving a low weight to pure shear regions that correspond to near wall regions in the global averaging, the predictions of the model are improved.

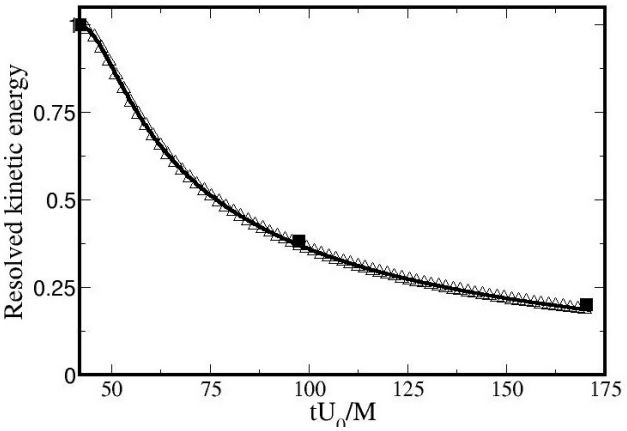


Figure 1. Resolved kinetic energy HIT of CBC on $64^3$ nodes. Triangle up GSIG, thick line GsvsSIG and the squares are the experiment.

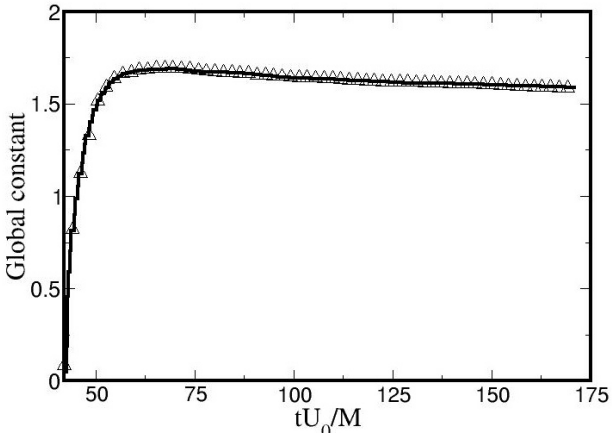


Figure 2. Global dynamic constant. Triangle up GSIG and solid line GsvsSIG.

## TOWARDS THE APPLICATION ON AN IMPINGING HOT JET ON ISOTHERMAL WALL

Accurate results were obtained in standard validation cases but it is necessary to assess the performance of this procedure in a more complex configuration that involves different flow features such as shear flows, rotations, stagnation points and unsteadiness To this respect, an experiment that consists in a pulsed hot jet that impinges on a cold surface in presence of a cross flow (at ambient temperature) was performed. This experiment was specially design for comparison with LES results purposes: simple enough to enable accurate model validation, fully controlled boundary conditions (the cross flow profile and injector profile were well-defined) and representative enough to take into account the most important physical phenomena occurring in combustion chambers: transient interactions between hot vortices and a developed boundary

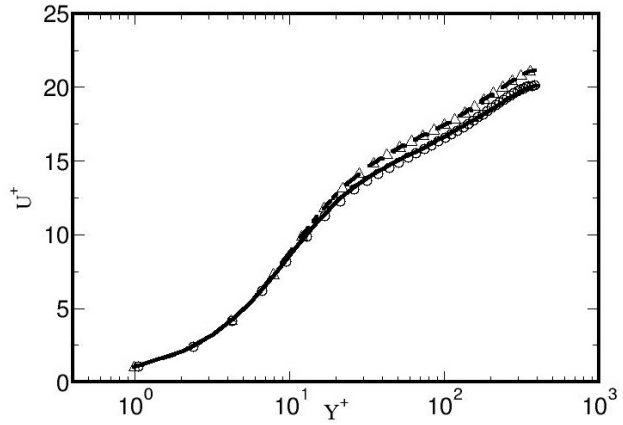


Figure 3. Mean velocity. Triangle up GSIG, solid line GsvsSIG, dashed line SMD and the circles are the DNS of Moser *et al.*

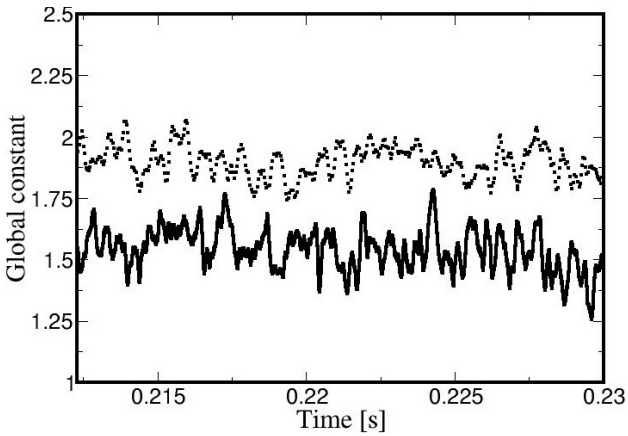


Figure 4. Global dynamic constant. Dotted line GSIG and solid line GsvsSIG.

layer. These guidelines led to the experimental set-up shown on Fig. 6 with the three main following characteristics: **1.** The global dimensions (nozzle hole, channel width) are consistent with the simulation constraints in order to allow full size computation of the geometry. In particular this led to the selection of the injector characterized by a large cross flow area together with a fast response time (of the order of 100 microseconds). **2.** The cross flow profile and turbulent characteristics are controlled by the use of inlet convergent and grid. The injector flow characteristics are also controlled by the use of a specific convergent profile, while the injection system is designed to control the upstream pressure. **3.** Wide optical access were provided by UV quality large quartz window in order to optimize the application of advanced optical diagnostics.

## Experimental set-up and PIV measurements

The pulsed jet is generated by an electric injector (fast response time and large flow area Hoerbiger GV50 injector) and the opening duration is about 10ms. The injection frequency is 1Hz. The injection diameter is d = 1cm. The impinging surface is situated at H = 2cm of the jet exit. The injector is supplied by a tank of volume V = 20l full of nitrogen. The nitrogen going to the injector is heated via an electric heater in order to keep it at the constant temperature. The nitrogen temperature at the exit of the jet was measured using a Two-color Toluene-LIF Imaging method (Tea *et al.*, 2011). The measured temperature at the jet exit is 343K. The air cross flow in the measuring section in which the mixing takes place is generated via a fan situated downstream. The cross flow is at ambient temperature. A convergent and a honeycomb situated upstream reduce significantly the fluctuation in the measurements section. The cross flow Reynolds number (based on the cross flow mean velocity and the channel width) is about 16000 and the jet flow Reynolds number (based on the mean inlet velocity and the injector's diameter) varies between 60000 and 12000.

PIV measurements were performed using a doubled frequency Nd:YAG-laser at 532nm. The signal was recorded with a CCD camera of 2048 X 2048 pixels resolution, equipped with a lens with the following characteristics: $f = 105mm$ and $f_{\#} = 2.8$. The time delay between the two pulses is 2 microseconds. Each pair of images was processed using cross correlation. Two preliminaries series of measurements were performed to get the initial conditions : a first one to characterize the injector flow rate (seeding inside the injector), the second one to characterize the cross flow turbulent intensity and mean profile (seeding only of the cross flow). The PIV measurements were performed on 3 plans in the streamwise direction ($Z$ direction at $Z = 0mm$,$7mm$, $15mm$ where the injector center is the origin) and 3 in the spanwise direction ($X$ direction at $X = -10mm$, $0mm$,$10mm$). For each plan, measurements were done at different times after the injection and the statistics were accumulated over 1000 snapshots.

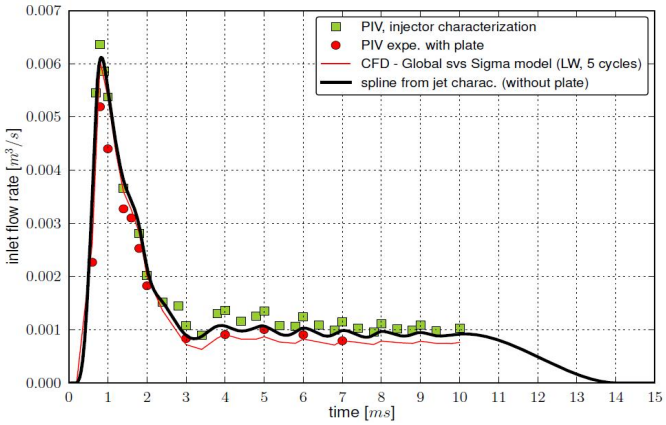


Figure 5. Flow rate. The plate corresponds to the impinging surface in presence of the cross flow.

## Numerical procedure and results

The numerical set-up of the experiment consisted in two steps. The first step was the cross flow modeling. This was done by initializing the same mean flow obtained with the PIV measurements with 1% turbulent intensity. Depending on the number of injections to perform, different cross flows solutions were used as initial conditions before the injection. This

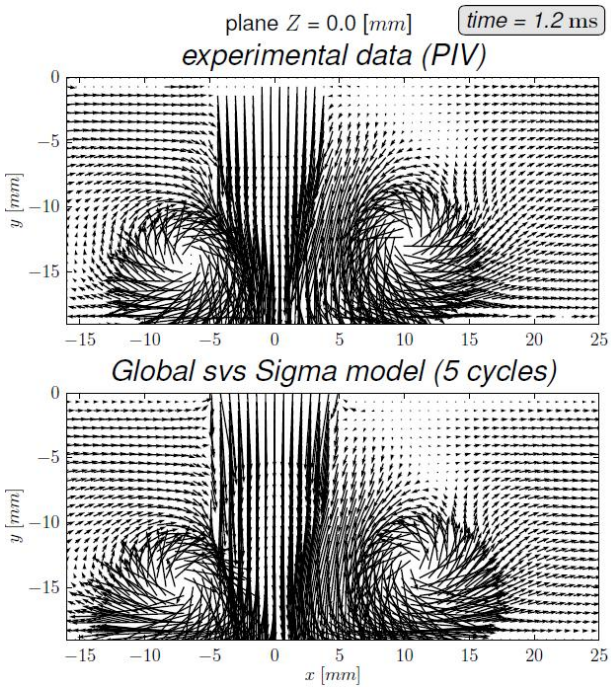


Figure 7. Velocity field at time 1.2$ms$ after the beginning of the injection. The cross flow comes from the left hand side.

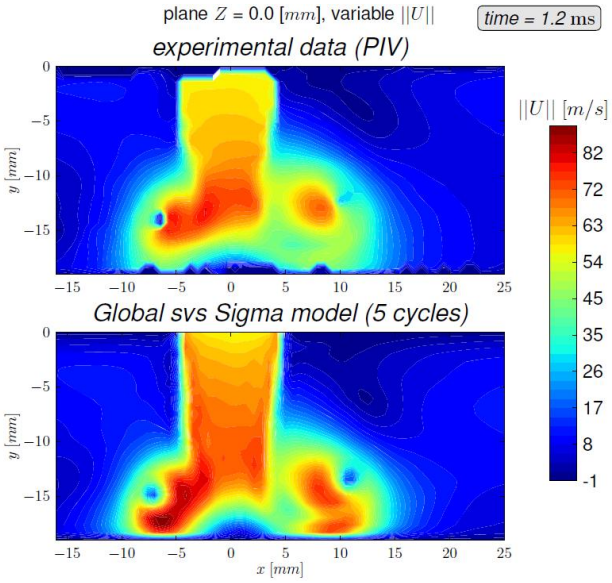


Figure 8. Velocity magnitude at time 1.2$ms$ after the beginning of the injection. The cross flow comes from the left hand side.

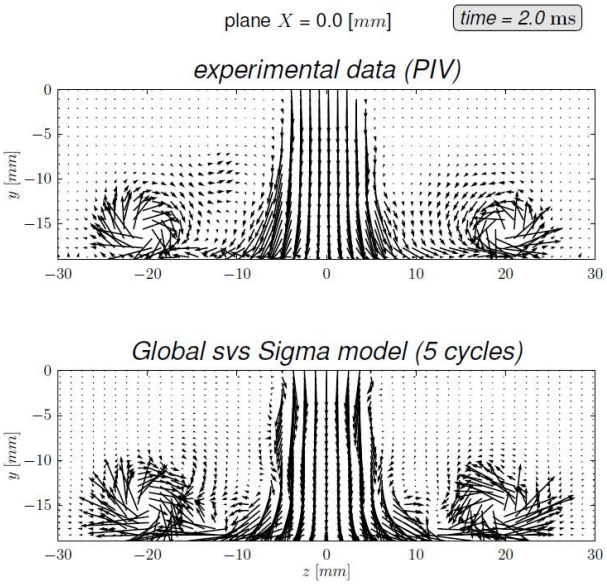


Figure 9. Velocity Field at time 2.0$ms$ after the beginning of the injection. Plan $X = 0$ perpendicular to the cross flow.

allows to have a different cross flow at each injection and to perform ensemble average if necessary. The target flow rate of the injector was obtained from the PIV measurements with cross flow rate turned off. The nitrogen inside the injector was initialized at the temperature obtained via LIF measurement and the solid boundaries of the convergent were kept at this temperature during the simulation. The other solid boundaries were maintained at ambient temperature with a noslip isothermal boundary condition.

The simulations were performed with a Lax-Wendroff finite volume numerical scheme that is second order accurate in space with a single time step integration. It has the advantage to be fast and it is commonly used for industrial applications. Fig 5 shows the different flows rate with and without cross flow for the experiment and the simulation. As expected in the experiment the flow rate decreases in presence of the cross flow. We can also observe that the flow rate obtained in the simulation with the cross flow is quite in good agreement with the experiments. It is worth noting that the inlet conditions have a major impact on the quality of the results of the simulations. The predictions of the simulation (averaged over 5 cycles/injections) at the impinging time ($t = 1.2ms$) are quite in good agreement with the PIV measurements as it can be seen on Fig 7 and Fig 9. The position of the vortex after the impingement is also well predicted as shown on Fig 9. Further comparison at various section are required to compare more accurately PIV measurements and simulations. However the concept of a global constant that varies only in time seems to lead to quite good results even in a complex configuration.

## CONCLUSION

The proposed modification for the global dynamic procedure allows to account for solid boundaries while keeping the interesting properties of the global approach. Indeed it does not require homogeneous directions nor clipping and it leads to same results in case of non wall bounded flows like an HIT. The combination with the $\sigma$-model provides accurate results on standard validation cases and on a more complex configurations that consists in a hot impinging unsteady jet with a cross flow. Although the constant is homogeneous in space and only varies in time, a first analysis shows that the

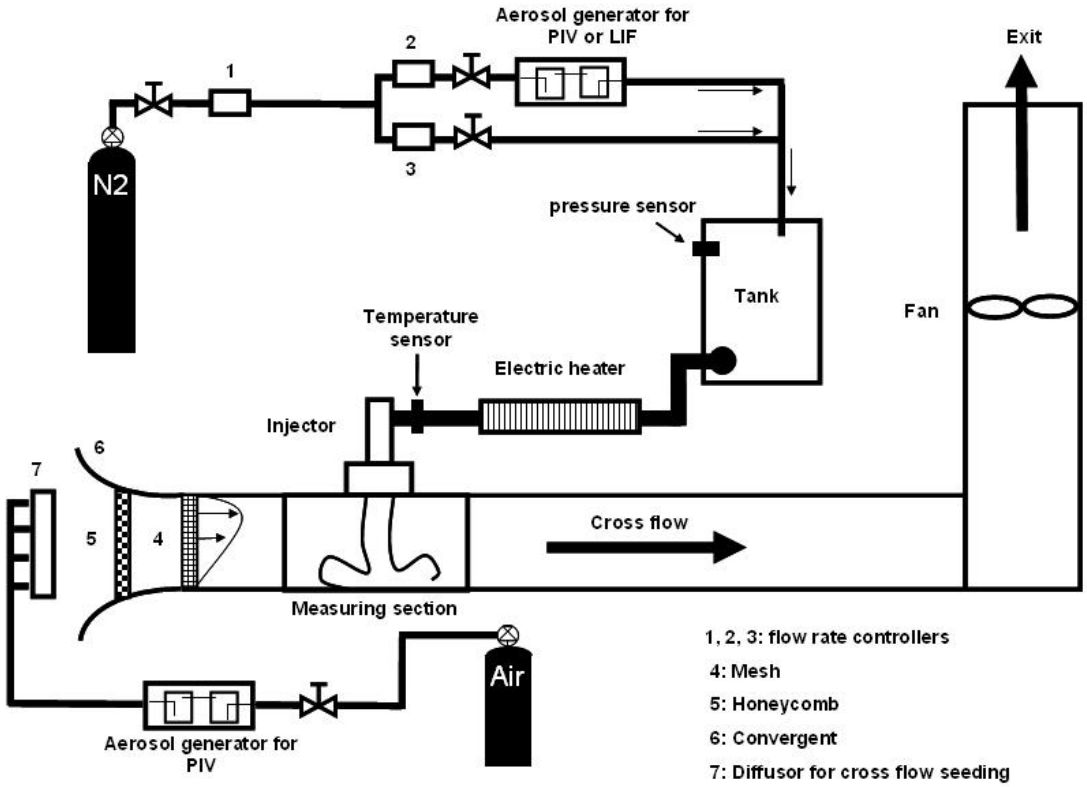


Figure 6. Schematic description of the experimental set-up of the hot impinging pulsed jet in presence of a cross flow.

simulation are in close agreement with the experiments. Further quantitative comparisons of the velocity field, the temperature stratification and rms still need to be done but the proposed procedure/model seems promising for extending the use of SGS models from simple academic cases to industrial applications.

## REFERENCES


AVBP 2011 *http://www.cerfacs.fr/4-26334-the-avbp-code.php.*

Baya Toda, H., Cabrit, O., Balarac, G., Nicoud, F. 2011 A subgrid-scale model based on singular values for LES in complex geometries. *In. Proceedings Center for Turbulence Research* NASA Ames/Stanford University.

Baya Toda, H., Truffin K., Nicoud, F. 2010 Is the dynamic procedure appropriate for all sgs models ? *In V European Conference on Computational Fluid Dynamics, ECCOMAS (ed. J.C.F. Pereira & A. Sequeira).*

Cabrit, O., Nicoud, F. 2009 Direct simulations for wall modelling of multicomponent reacting compressible turbulent flows. *Physics of Fluids* **21**(055108).

Comte-Bellot, G., Corsin, S. 1971 Simple Eulerian time correlation of full narrow-band velocity signals in grid generated "isotroppic" turbulence. *Journal of Fluid Mechanics* **48**, 273-337.

Germano, M. and Piomelli, U. and Moin, P. and Cabot, W. 1991 A dynamic subgrid-scale eddy viscosity model *Physics of Fluids* **3** 1760-1765.

Kim, J., Moin, Moser, R. 1987 Turbulence statistics in fully developed channel flow at low Reynolds number *Journal of Fluid Mechanics* **177** 133-166.

Lee, J., Choi, H., Park, N. 2010 Dynamic global model for large-eddy simulation in transient flows. *Physics of fluids* **22, 075106**.

Lilly, D. K. 1992 A Proposed Modification of the Germano Subgrid-Scale Closure Method. *Physics of fluids* **A4(3)** 633-635.

Nicoud, F., Ducros, F. 1999 Subgrid-scale stress modeling based on the square of the velocity gradient tensor. *Flow, Turbulence and Combustion* **62** 183-200.

Nicoud, F., Baya Toda, H., Cabrit, O., Bose, S., Lee, J. 2011 Using singular values to build a subgrid-scale model for Large Eddy Simulations. *submitted to Physics of Fluids.*

R. D. Moser, J. Kim, Manssour, N. N. 1999 Direct numerical simulation of turbulent channel flow up to $Re_\tau = 590$. *Physics of fluids* **11(4)**.

Smagorinsky, J. 1963 General circulation experiments with the primitive equations. *Month. Weather* **93** 99-165.

Tea, G., Bruneaux, G., Kashdan, J.T., Schulz, C. 2011 Unburned gas temperature measurements in a surrogate Diesel Jet via Two-color Toluene-LIF imaging. *Proceeedings of the Combustion Institute* **33** 783-780.

Vreman, A. 2004 An eddy-viscosity subgrid-scale model for turbulent shear flow : Algebraic theory and applications. *Physics of fluids*. **16(10)**.